Number1 Volume 13 march 2007 Journal of Engineering

HELICAL WINDING INDUCTION HEATING SYSTEM

J. H. H. Alwash, Ph. D, C. Eng., M. IEE, M. IEEE
and L. J. B. Qasir, M. Sc., Ph. D.

ABSTRACT
A novel method in induction heating is presented. The winding of the excitation coil is helical and of three – phase type while the charge is cylindrical. This heating system is compared with the classical induction heating system of the circular coil type with cylindrical charge and single – phase excitation. The study shows the merits of the proposed new system over the conventional one. The multi – layer theory approach is adopted for the analysis of helical winding induction heating system which is an analytical method.

الخلاصة

يتناول هذا البحث دراسة اسلوب جديد للتسخين بالحث الكهرومغناطيسي باستخدام ملفات لولبية ثلاثية الطور ذات شحنة اسطوانية الشكل و بناء نموذج رياضي لها. تتضمن الدراسة دراسة مزايا اسلوب التسخين الجديد بالمقارنة مع ملفات التسخين التقليدية احادية الطور بلفافها الدائرية و المحيطة بذات الشنة الاسطوانية و ذلك من خلال حساب مواصفات المنظومة مثل المقاومة، القدرة المحتثة في الشحنة و الكفاءة. تم استخدام طريقة تحليلية صرفة و هي نظرية الطبقات بالنسبة للمنظومة الجديدة ذات الملفات اللولبية اما بالنسبة للمنظومة التقليدية فقد تم تحليلها باستخدام طريقة الدائرة المكافئة.

KEY WORDS
Helical winding, induction heating.

INTRODUCTION

Three – phase induction heating systems are normally known as traveling wave induction heaters [1] . When the metallic charge is held stationary, the induced currents will heat it which can now be regarded as the workpiece. The method has uses in vessel and billet heating. The diffusion of the time – variable electromagnetic field in the conduction media is accompanied by electrothermal and electromagnetic effects. Some technical applications are based on the dynamic effect, for example, the electromagnetic stirring in traveling low frequency magnetic field, for steel degassing and treatment [2] .

Fireteanu and Gheysens [3] presented a comparison between single phase and travelling wave induction heating system for crucible furnace. They concluded that the electromagnetic stirring of the molten metal by the action of electromagnetic force was more intensive in the case of travelling wave induction with a reduction of active power by an amount (8 – 23) %. The objective of this paper is to propose a mathematical model for the travelling wave helical winding induction heating system with poles distributed axially and circumferentially. A second objective of this paper is to compare the results of the helical model with those obtained for the conventional model and to show the merits of the new system over the conventional one.

For the analysis, a conventional system is adopted from reference [1] for the sake of comparison. The model is a system operating in the standard frequency (50 Hz). The results of helical system are compared with those obtained for the single – phase system obtained by the equivalent circuit method [(1)] .

Winding Layout

The basic development of the helical winding can be explained with the aid of **fig. (1)**. **Fig. (1 – a)** shows a flat layout of the instantaneous pole pattern of a HWIH system. If this layout is rolled about an axis and applied (EE) to (FF), the result is a helical travelling wave induction heating system as shown in **fig. (1 – b).**

The primary coil construction of one phase of the winding may be explained with the aid of **fig. (2). Fig. (2 – a)** shows the coil structure for planner heater. To convert this into the cylindrical shape, it is rolled to produce the construction shown in **fig. (2 – b)**. Polyphase versions of the winding may of course be arranged.

Fig. (3) shows unrolled three – phase configuration; with two poles circumferentially and axially. **Fig. (4)** shows the helical windings in cylindrical form for two poles axially.

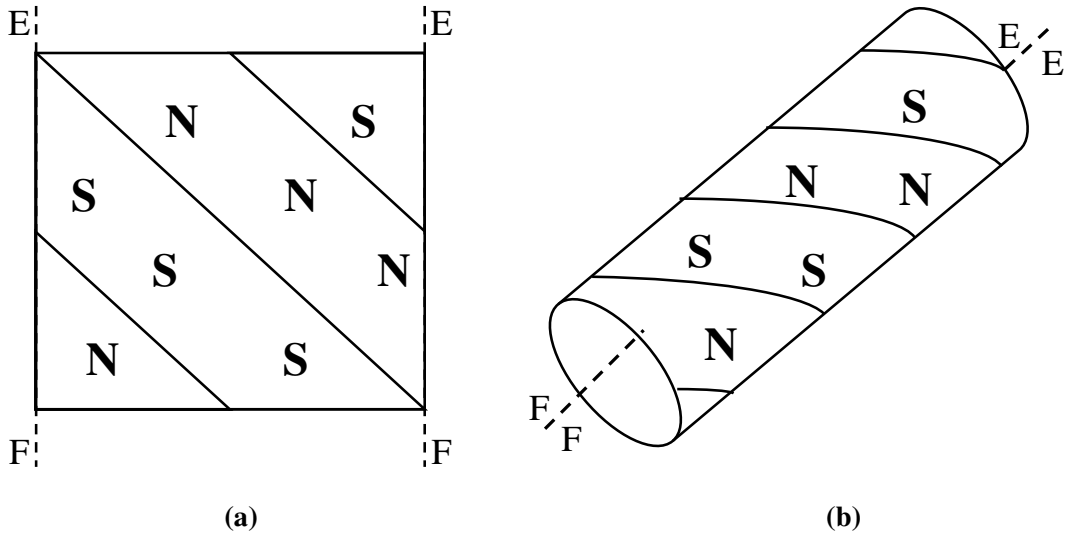

(a) **(b)**

Fig. (1).
Basic development of the helical winding
(a) A flat layout of the instantaneous pole pattern of a HWIH system
(b) A helical travelling wave induction heating system

THEORETICAL ANALYSIS

Primary current density

It is assumed that the winding produce perfect sinusoidal travelling wave. The line current density may be represented by[(4)]:

$$J = J_s \exp j(\omega t - kz + n\theta) \qquad (1)$$

where

$$J_s = J_m \exp(j\phi)$$

$$\phi = \tan^{-1}\frac{n}{k \cdot r_g}$$

$$k = \frac{\pi \cdot \cos(\phi)}{p}$$

and

$$J_m = \frac{N_c I_m}{W_c}$$

This may be resolved into two components, J_z and, J_θ where:

$$J_z = J_{zm} \exp j(\omega t - kz + n\theta) \quad (2)$$

$$J_\theta = J_{\theta m} \exp j(\omega t - kz + n\theta) \quad (3)$$

and:

$$J_{zm} = J_m \sin(\phi)$$

$$J_{\theta m} = J_m \cos(\phi)$$

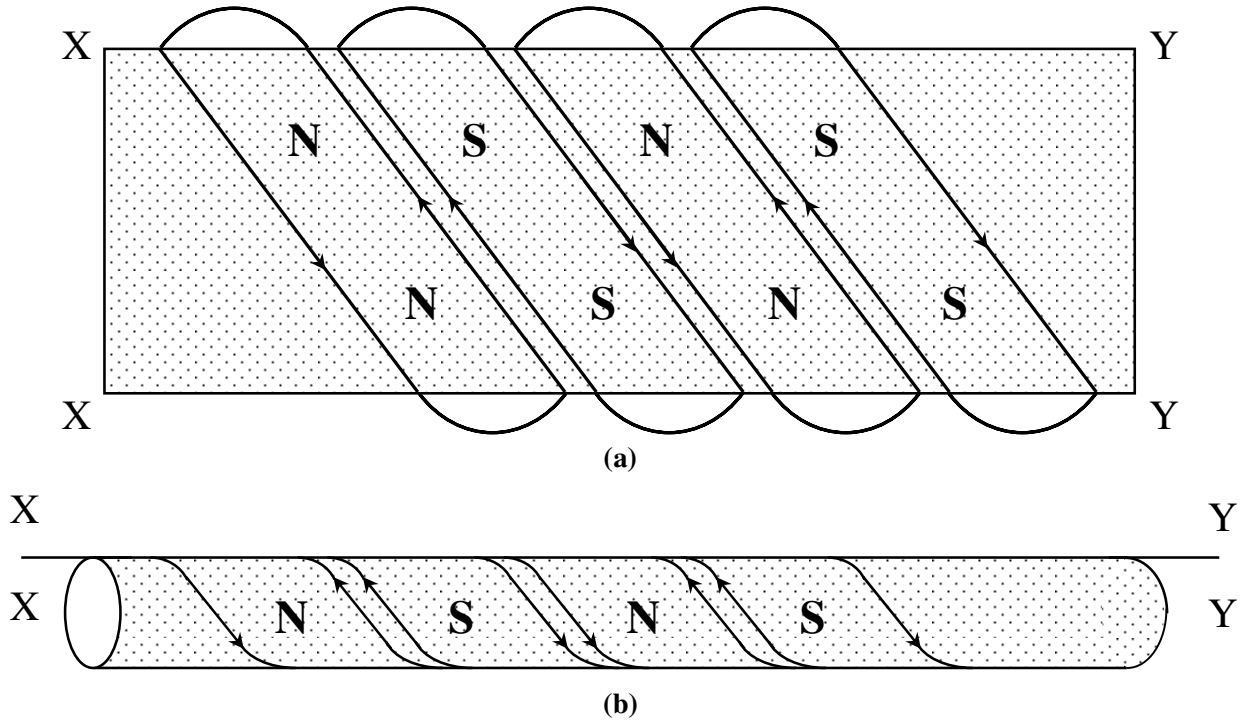

Fig. (2).
Primary – coil construction for one phase of the HWIH
(a) Coil structure of figure (1 – a)
(b) Coil structure of figure (1 – a) in cylindrical shape

Mathematical model

A general multi – region problem is analyzed. **Fig. (5)** shows a longitudinal section in HWIH system. **Fig. (6)** shows a cross – section through the model shown in **fig. (5)**. This represented the general mathematical model chosen for the analysis. The solution is based on the following assumptions:

1. The primary current is represented by a radially infinitesimally thin and axially infinite current sheet excitation at radius r_g .
2. All state variables vary sinusoidally as $\exp j(\omega t - kz + n\theta)$. This exponential will be dropped from the expression for shortness.
3. All field components decay to zero at sufficiently far radial distances from the model.
4. Displacement currents will be neglected at the frequencies used.

Maxwell's equations for any region in the model are:

$$\nabla \times \overline{H} = \overline{J} \tag{4}$$

$$\nabla \times \overline{E} = \frac{-\partial \overline{B}}{\partial t} \tag{5}$$

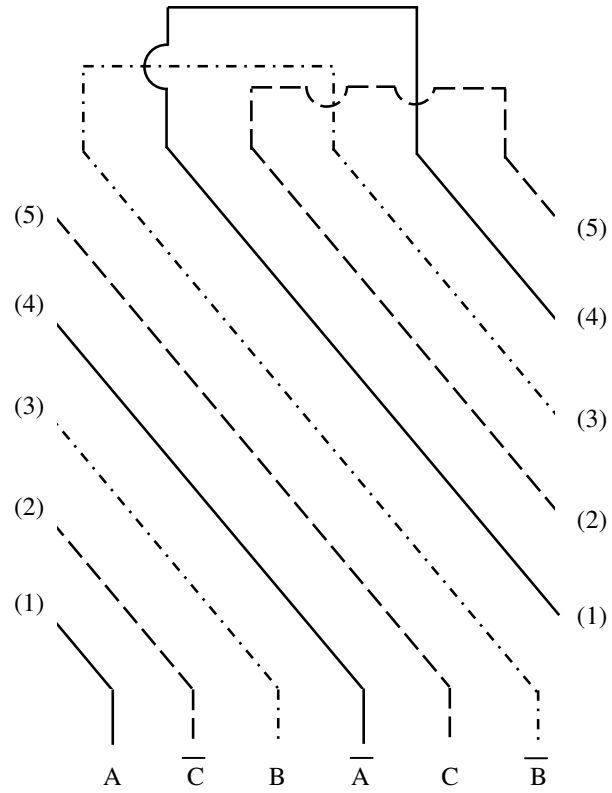

Fig. (3).

A flat layout of unrolled 3 – phase HWIH with two poles axially and circumferentially

$$\nabla \cdot \overline{B} = 0 \tag{6}$$

$$\nabla \cdot \overline{J} = 0 \quad (7)$$

$$\nabla \cdot \overline{E} = 0 \quad (8)$$

$$\overline{J} = \sigma \overline{E} \quad (9)$$

$$\overline{B} = \mu \overline{H} \quad (10)$$

It is assumed that the resistivity in the radial direction is infinite, this gives:

$$J_r = 0 \quad (11)$$

The boundary conditions are:

1. The axial flux density is continuous across a boundary.
2. The axial component for magnetic field strength is continuous across a boundary, but allowance must be made for the current sheet in the manner shown in the section concerning field calculation at the region boundaries.

Field equation of a general region

Firstly, the field components of a general region are derived. Assuming that $\sigma_z = \sigma_\theta = \sigma$ and $\mu_r = \mu_\theta = \mu_z = \mu$, then using equation (7), for $n \neq 0$, we have:

$$J_z = \frac{n}{r.k} J_\theta \quad (12)$$

Using equation (9) yields:

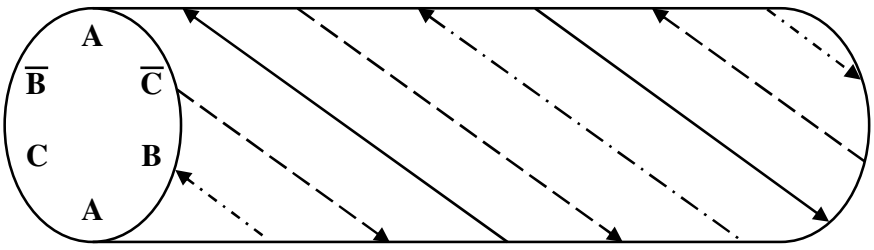

Fig. (4).
Helical winding in cylindrical form for two poles axially

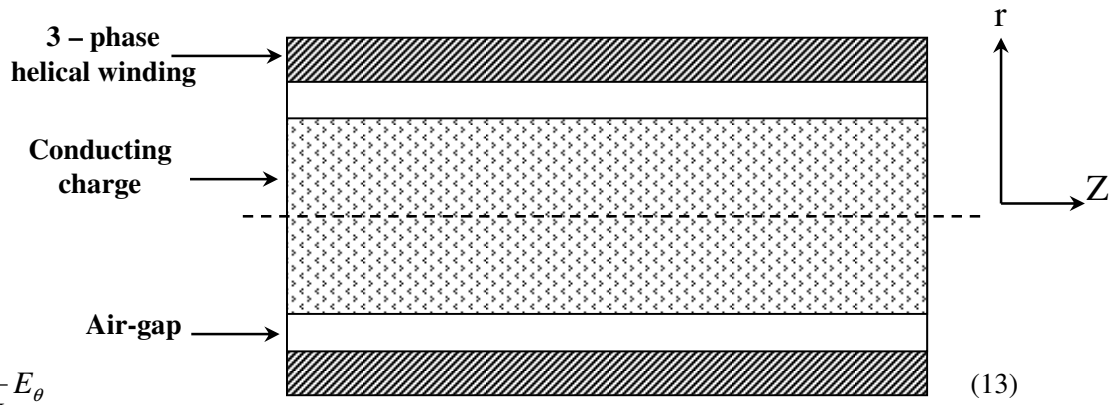

$$E_z = \frac{n}{r.k} E_\theta \tag{13}$$

From equations (5), (4) and (9):

$$\nabla \times \nabla \times \overline{E} = -j\omega\sigma\mu\overline{E} \tag{14}$$

Taking only the z – components from both sides of equation (14) and using equation (8) with the assumptions mentioned above, the general solution is:

$$E_z = A.I_n(\alpha r) + D.K_n(\alpha r) \tag{15}$$

Where:

$$\alpha^2 = k^2 + j\omega\mu\sigma \tag{16}$$

I_n and K_n are modified Bessel functions of order n and of general complex argument. *A* and *D* are arbitrary constants to be determined from boundary conditions.

From equation (13) and equation (15), for $n \neq 0$,

$$E_\theta = \frac{r.k}{n}\left[A.I_n(\alpha r) + D.k_n(\alpha r)\right] \tag{17}$$

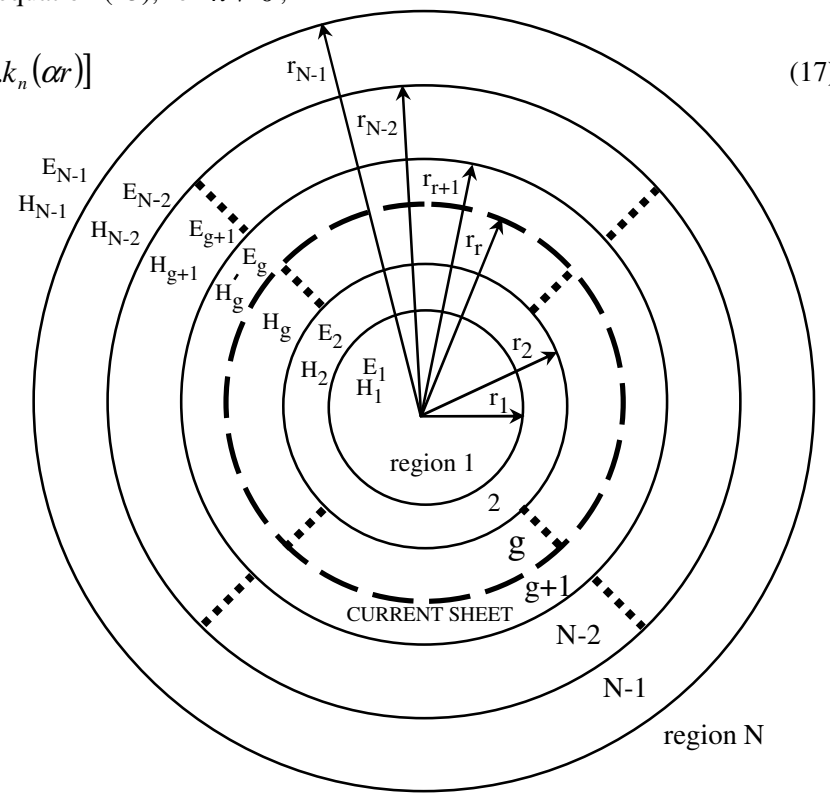

Fig. (6).

Cross – section through multicylindrical induction heater
Note: The dotted lines describe region(s) in between
Using equations (5), (9), (13) and (15), it can be shown that:

$$H_r = -\left(\frac{n^2 + k^2 r^2}{\omega \mu r^2 k}\right) E_\theta \tag{18}$$

Using equation (4) and equation (11), taking only the r – component, yields:

$$H_\theta = -\frac{n}{r.k} H_z \tag{19}$$

Using equations (6), (10), (17), (18) and (19)

$$H_z = \frac{jr.k}{n\omega\mu}\left[\left(\frac{2r.k^2}{n^2 + r^2k^2} - \frac{n}{r}\right)\left(A.I_n(\alpha r) + D.K_n(\alpha r)\right) + \alpha\left(A.I_{n-1}(\alpha r) - D.K_{n-1}(\alpha r)\right)\right] \tag{20}$$

Field calculation at the region boundaries

Fig. (7 – a) shows a general region m, where $E_{\theta,m}$ and $H_{z,m}$ are the field components at the upper boundary of region m, and $E_{\theta,m-1}$ and $H_{z,m-1}$ are the equivalent values at the lower boundary of the same region. From equation (17) and equation (20), we may write:

$$E_{\theta,m} = \frac{r_m.k}{n}\left[A.I_n(\alpha_m r_m) + D.K_n(\alpha_m r_m)\right] \tag{21}$$

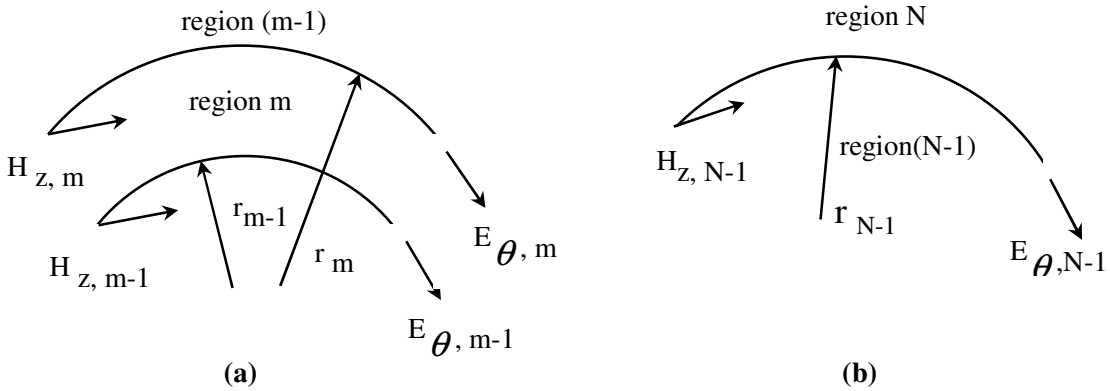

(a)
Mathematical model for general region m

(b)
Mathematical model for end region N

Fig. (7).
Mathematical model

$$H_{z,m} = \frac{jr_m.k}{n\omega\mu_m}\left[\left(\frac{2r_m.k^2}{n^2 + r_m^2k^2} - \frac{n}{r_m}\right)\left(A.I_n(\alpha_m r_m) + D.K_n(\alpha_m r_m)\right)\right.$$
$$\left. + \alpha_m\left(A.I_{n-1}(\alpha_m r_m) - D.K_{n-1}(\alpha_m r_m)\right)\right] \quad (22)$$

Expressions for $E_{\theta,m-1}$ and $H_{z,m-1}$ can be found by replacing r_m in the above equations by r_{m-1}.

For regions where $m \neq 1$ or N

$$\begin{bmatrix} E_{\theta,m} \\ \\ H_{z,m} \end{bmatrix} = \begin{bmatrix} \\ T_m \\ \\ \end{bmatrix}.\begin{bmatrix} E_{\theta,m-1} \\ \\ H_{z,m-1} \end{bmatrix} \quad (23)$$

Where $[T_m]$ is the transfer matrix [5] for region m, and is given by:

$$\begin{bmatrix} \\ T_m \\ \\ \end{bmatrix} = \begin{bmatrix} a_m & b_m \\ \\ c_m & d_m \end{bmatrix} \quad (24)$$

Expressions for a_m, b_m, c_m and d_m are given in reference (4)

At the boundaries where no excitation current sheet exists, E_θ and H_z are continuous. Considering the current sheet to be at radius r_g, then:

$$H'_{z,m} = H_{z,m} \quad , \quad m \neq g \quad (25)$$

And

$$H'_{z,m} = H_{z,m} - J_\theta \quad , \quad m=g \quad (26)$$

Where $H_{z,m}$ is the axial magnetic field strength immediately below a boundary and $H'_{z,m}$ is the axial magnetic field strength immediately above a boundary. Hence it can be written that:

$$\begin{bmatrix} E_{\theta,N-1} \\ \\ H_{z,N-1} \end{bmatrix} = \begin{bmatrix} \\ T_{N-1} \\ \\ \end{bmatrix}\begin{bmatrix} \\ T_{N-2} \\ \\ \end{bmatrix}\ldots\begin{bmatrix} \\ T_{g+1} \\ \\ \end{bmatrix}\begin{bmatrix} E_{\theta,g} \\ \\ H_{z,g} - J_\theta \end{bmatrix} \quad (27)$$

And

$$\begin{bmatrix} E_{\theta,g} \\ \\ H_{z,g} \end{bmatrix} = \begin{bmatrix} \\ T_g \\ \\ \end{bmatrix} \begin{bmatrix} \\ T_{g-1} \\ \\ \end{bmatrix} \ldots \begin{bmatrix} \\ T_2 \\ \\ \end{bmatrix} \begin{bmatrix} E_{\theta,1} \\ \\ H_{z,1} \end{bmatrix} \tag{28}$$

For region N, **fig. (7 – b)**, then as $r \to \infty, I_n(\alpha r) \to \infty$, from equations (21) and (22):

A=0

$$E_{\theta,N-1} = \frac{r_{N-1}.k}{n}\left[D.K_n(\alpha_N r_{N-1})\right] \tag{28}$$

And

$$H_{z,N-1} = \frac{jDr_{N-1}k}{n\omega\mu_N}\left[\left(\frac{2r_{N-1}.k^2}{n^2 + r_{N-1}^2 k^2} - \frac{n}{r_{N-1}}\right)K_n(\alpha_N r_{N-1}) - \alpha_N K_{n-1}(\alpha_N r_{N-1})\right] \tag{29}$$

For region 1, as $r \to 0, K_n(\alpha r) \to \infty$, therefore, from equations (21) and (22):

D = 0 (30)

$$E_{\theta,1} = \frac{r_1.k}{n}\left[A.I_n(\alpha_1 r_1)\right] \tag{31}$$

$$H_{z,1} = \frac{jAr_1k}{n\omega\mu_1}\left[\left(\frac{2r_1.k^2}{n^2 + r_1^2 k^2} - \frac{n}{r_1}\right)I_n(\alpha_1 r_1) - \alpha_1 I_{n-1}(\alpha_1 r_1)\right] \tag{32}$$

Surface impedance calculations

The surface impedance looking outwards at a boundary of radius (r_g) is defined as:

$$Z_{g+1} = \frac{E_{\theta,g}}{H'_{z,g}} \tag{33}$$

And the surface impedance looking inwards is defined as:

$$Z_g = \frac{-E_{\theta,g}}{H_{z,g}} \tag{34}$$

Using the methods obtained in reference [6] with the values of $E_{\theta,N-1}, H_{z,N-1}, E_{\theta,1}, H_{z,1}$ and a_m, b_m, c_m and d_m as derived in the previous section, then:

$$Z_{in} = \frac{Z_g.Z_{g+1}}{Z_g + Z_{g+1}} \tag{35}$$

Where Z_{in} is the input surface at the current sheet and Z_{g+1} and Z_g are the surface impedances looking outwards and inwards at the current sheet. Substituting for Z_g and Z_{g+1} using equation (34) and equation (33) respectively and rearranging gives:

$$Z_{in} = \frac{-E_{\theta,g}}{H_{z,g} - H'_{z,g}} \tag{36}$$

Using eqation (26),

$$H'_{z,g} = H_{z,g} - J_\theta$$

Substituting this in equation (36),

$$Z_{in} = \frac{-E_{\theta,g}}{J_\theta}$$

Thus, the input surface impedance at the current sheet has been determined. This means that all field components can be found by making use of this and equations (34), (27) and equation (28).

Power calculation

The time – average power flowing through a boundary is given as [7]:

$$P = \mathrm{Re}\left\{\frac{1}{2\pi}\int_0^\pi \left(E_\theta H_z^* - E_z H_\theta^*\right) d\theta\right\} \qquad W/m^2 \tag{37}$$

Using equations (13), (18), (28) and the concept of surface impedance [6,7] it can be shown that:

$$P_{in} = \pi . r_g \left[1 + \left(\frac{n}{k.r_g}\right)^2\right] |J_\theta|^2 \,\mathrm{Re}\{Z_{in}\} \quad \text{W/m} \tag{38}$$

NUMERICAL RESULTS

A model from reference[1] is adopted. The computations are made using the equivalent circuit method for the conventional system and layer theory approach for helical system. The operating frequency is 50 Hz and the helical winding is connected for two poles axially and two poles circumferentially. **Table (1)** shows the data for both systems. The number of turns for helical system is chosen such that equal coil losses are obtained for both systems. It should be noted that turn length for helical system is given by [8]:

$$l_H = 2\pi d_{av}\left(\frac{1}{\cos\phi} + \frac{\pi}{4n}\right), \quad \text{meter} \tag{39}$$

Where:

l_H : Average helical turn length.

d_{av}: Average coil diameter.

ϕ: Helicoid angle at the inner coil radius.

And the coil efficiency is given by [1] :

$$\eta = \frac{R_W}{R_W + R_C} \tag{40}$$

Where:

R_W: charge resistance per phase (Ω).

R_C: coil resistance per phase (Ω).

Table (2) shows a comparison between the two systems. The computations were made using the equivalent circuit method for the conventional system and layer theory approach for helical system.

Table (1)
Data for helical system and conventional system

Parameter	Value
Number of axial poles	2
Number of circumferential poles	2
Coil inner radius (mm)	87.5
Axial coil length (mm)	2000
Turns per coil for helical system	2
Number of turns for conventional system	54.7
Axial pole pitch (mm)	1000
Helicoid angle on primary (degree)	68.17
Normal pole pitch (mm)	371.85
Normal slot pitch (mm)	123.95
Normal coil width (mm)	42.76
Slots per pole per phase	1
Exciting phase current (Amp.)	12160
Frequency (Hz)	50
Conductivity of coil conductor (mho/m)	5.066×10^7
Outer charge radius (mm)	75
Charge conductivity (mho/m)	1.86916×10^7
Charge relative permeability	1

Table (2)
Comparison between helical and conventional system parameters

Parameter	Equivalent circuit method for conventional system	Layer theory approach for helical system
Charge power (kw)	307	739.3
Per phase charge resistance (m Ω)	2	1.67
Coil efficiency %	60.29	78.5

The coil conductor is hollow for cooling purposes and has rectangular shape, **fig. (8)**. In this case two turns are used in each phase, the turns are assembled either axially beside each other or radially one above the other and therefore there are two conductor sizes. **Table (3)** shows the conductor size for the two cases of helical system together with the water cooling circuit parameters.
Figs. (9), **(10) and (11)** show the variation of radial, circumferential and axial flux density components with charge radius for both conventional and helical system at 50 Hz. The figures show that while there is only one component for the conventional system which is the axial one (the radial component being zero, the circumferential component is zero due to circular symmetry), the helical system has all components, it is worth noting that the magnitude of total flux density is greater for helical system. It is shown that flux density components are maximum at outer charge radius and decay exponentially as the radius approaches zero due to skin effect. **Fig. (12)** shows the charge power against frequency for both systems. It is evident that power is greater in the case helical system.

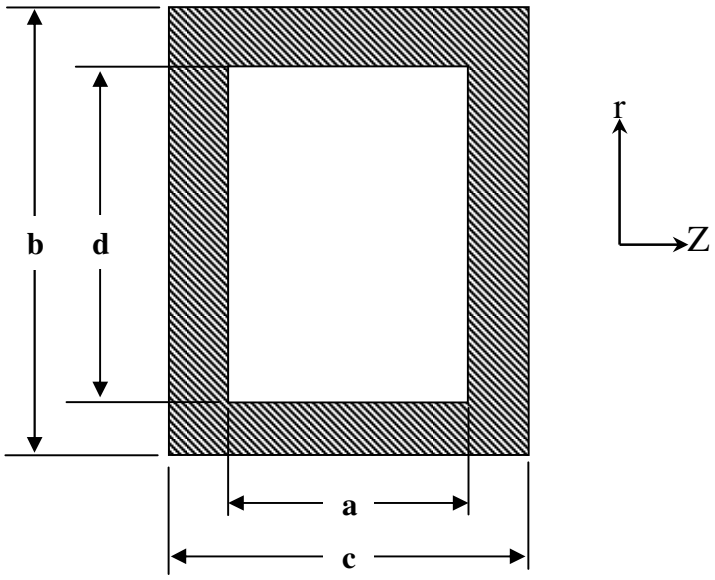

Fig. (8).
A cross section in a coil conductor

Table (3)
Two conductor dimensions arrangement of helical system with water circuit parameters

Parameter	The two conductors one above the other	The two conductors one beside the other
a (mm)	30	12
b (mm)	35	80
c (mm)	20	7
d (mm)	25	60
Radiation power (kw)	0.96	0.96
Coil power (kw)	198.7	202.4
Water temperature rise (^0C)	30	30
Water flow rate (lit/min)	94.6	96.4
Water velocity (m/sec)	3.15	3.82
Water pressure drop (bar)	1.61	4.6

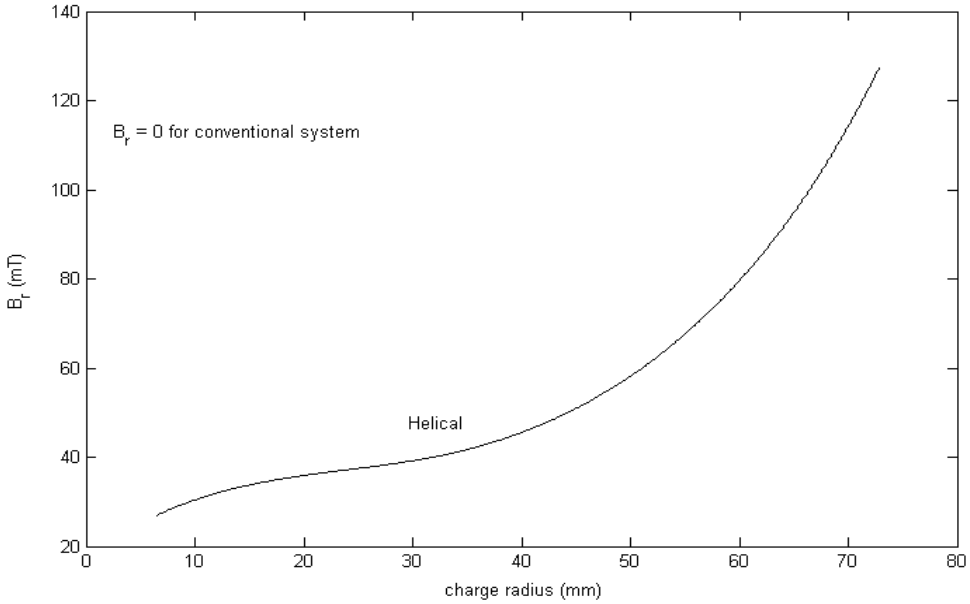

Fig. (9).
Radial flux density distribution along charge radius

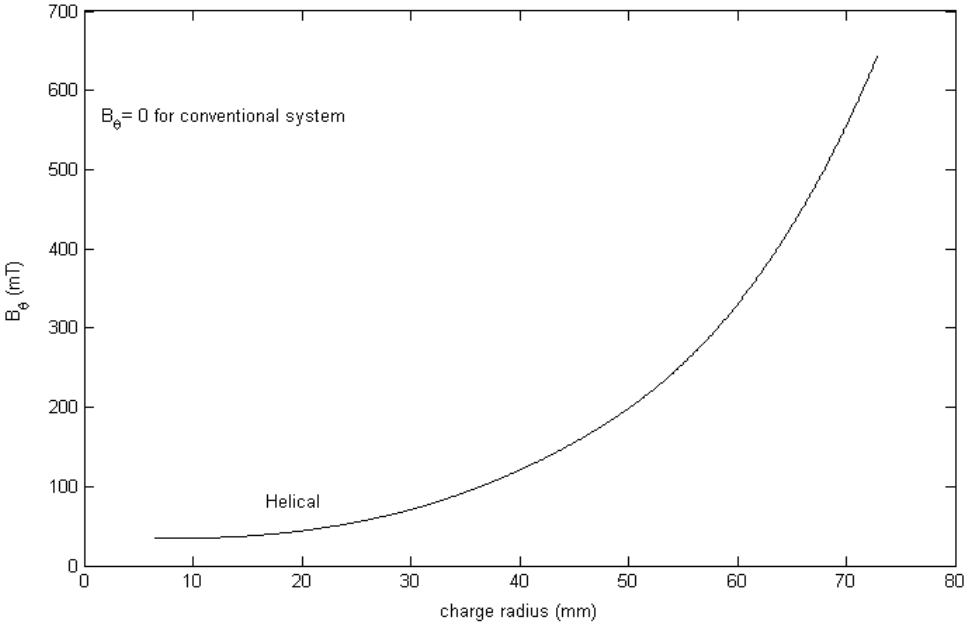

Fig. (10).
Circumferential flux density distribution along charge radius

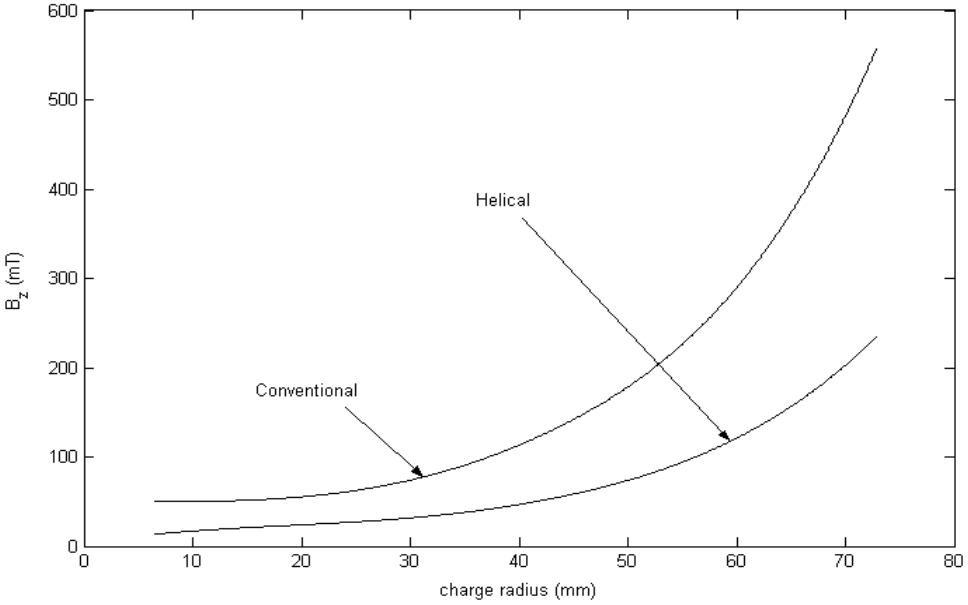

Fig. (11).
Axial flux density distribution along charge radius

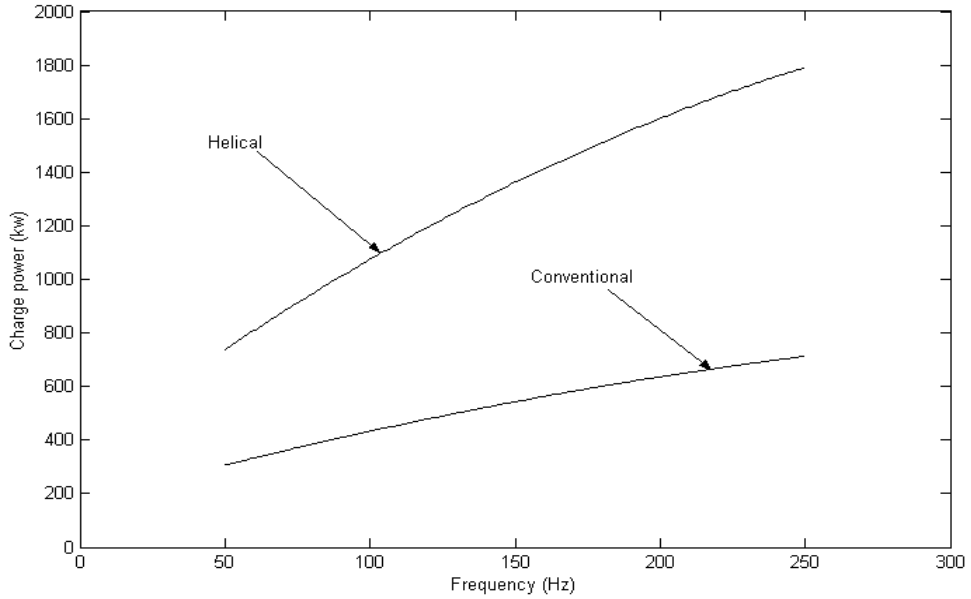

Fig. (12).
Variation of charge power against frequency

CONCLUSIONS

A novel method for three – phase induction heating with cylindrical charge is presented. This system is compared with conventional model taken from reference [1]. It is revealed that higher induced power in the charge is obtained with the helical system for same coil losses, hence higher heating efficiency and lower heating time.

REFERENCES

1. Daves, J. and Simpson, P.; "Induction heating hand book", McGraw – Hill Book Company, (UK), 1979.
2. Sundberg Y., "Principle of induction stirrer", ASEA Journal, 4, 1971.
3. Fireteanu, V. and Gheysens, R., "Numerical modeling of the travelling field diffusion. Induction heating and electromagnetic stirring", ibid, Vol. 28, No. 2, Mar. 1992, pp. 1489 – 1492.
4. Alwash, J. H. H., Mohssen, A. D. and Abdi, A. S.; "Helical motion tubular induction motor", IEEE Trans. On Energy conversion, Vol. 18, No. 3, PP. 362 – 369, Sept. 2003.
5. Greig, J., and Freeman, E. M., "Travelling wave problem in electrical machines", Proc. IEE., Vol. 114, No. 11, pp. 1681 – 1683, Nov. 1967.
6. Freeman, E. M. and Smith, B. E., " Surface impedance method applied to multilayer cylindrical induction devices with circumferential exciting currents", Proc. IEE, Vol. 117, No. 10, pp. 2012 – 2013, Oct. 1970.
7. Alwash, J. H.; "Analysis and design of linear induction machines"; Ph.D. Thesis, Imperial College, London University, U. K., 1972.
8. Abdi, A. S.;" Performance study of helical winding tubular linear induction motor"; M. Sc. Thesis, College of engineering, University of Baghdad, Baghdad, 1999.